Biochemical and Biophysical Research Communications 380 (2009) 160–165

Contents lists available at ScienceDirect

Biochemical and Biophysical Research Communications

journal homepage: www.elsevier.com/locate/ybbrc

NMR structure of the Wnt modulator protein Sclerostin

Stella E. Weidauer [a], Peter Schmieder [b], Monika Beerbaum [b], Werner Schmitz [c], Hartmut Oschkinat [b], Thomas D. Mueller [a,*]

[a] Lehrstuhl für Botanik I-Molekulare Pflanzenphysiologie und Biophysik, Julius-von-Sachs Institut für Biowissenschaften (Biozentrum) der Universität Würzburg, Julius-von-Sachs Platz 2, D-97082 Würzburg, Germany
[b] Leibnitz-Institut für Molekulare Pharmakologie, Robert-Rössle-Str.10, D-13125 Berlin, Germany
[c] Lehrstuhl für Physiologische Chemie II, Theodor-Boveri Institut für Biowissenschaften der Universität Würzburg, Am Hubland, D-97074 Würzburg, Germany

ARTICLE INFO

Article history:
Received 2 January 2009
Available online 21 January 2009

Keywords:
SOST
NMR structure
LRP5
Wnt antagonist
Cystin-knot
Bone metabolism

ABSTRACT

Sclerostin has been identified as a negative regulator of bone growth. Initially it was considered that Sclerostin performs its regulatory function via acting as a modulator of bone morphogenetic proteins (BMPs) similar to known examples such as Noggin, Chordin, and members of the DAN family. Recent findings, however, show that Sclerostin interferes with the Wnt signaling pathway due to binding to the Wnt co-receptor LRP5 thereby modulating bone growth. As Sclerostin is exclusively produced by osteocytes located in bones, neutralization of its bone-inhibiting functions makes it a highly interesting target for an osteoanabolic therapeutic approach in diseases characterized by bone loss, such as osteoporosis. Despite the huge interest in Sclerostin inhibitors the molecular basis of its function and its interaction with components of the Wnt signaling cascade has remained unclear. Here, we present the NMR structure of murine Sclerostin providing the first insights how Sclerostin might bind to LRP5.

The bone mass disorders Sclerosteosis and van Buchem disease are two rare but severe inherited disorders characterized by a phenotype of progressive bone thickening due to massively increased bone formation [1,2]. Both autosomal recessive diseases are caused by inactivating mutations in the *SOST* gene. Whereas in Sclerosteosis missense mutations in the coding region were identified, a deletion in an enhancer region downstream of the *SOST* gene is causative for the van Buchem disease [3,4]. The *SOST* gene encodes for the secreted protein Sclerostin (SOST) [5]. One feature of the protein is the presence of a cystin-knot motif, which allocates SOST into the DAN family. This family comprises several members, e.g. Gremlin, DAN, Cerberus, which have been described as BMP and/or TGF-β antagonists. However, amino acid similarity of SOST to the members of the DAN family is rather limited. The expression of SOST in the adult organism is restricted to the bones, where SOST is expressed and secreted by osteocytes and acts as a negative regulator of osteoblast development and bone formation [6–9]. Early studies proposed SOST might act as a direct BMP antagonist [8], however, accumulating evidence suggests Sclerostin as a modulator of the canonical Wnt signaling pathway. SOST binds to the Wnt co-receptor LRP5/6 thereby inhibiting Wnt signaling [10,11]. Conformingly mutations in the *lrp5* gene causing the High Bone Mass phenotype, which is similar to the phenotype of Sclerosteosis and van Buchem disease, show decreased binding to SOST [12,13].

Inhibition of Sclerostin should lead to increased bone density making SOST a perfect drug target for the development of an osteoanabolic therapeutic agent against osteoporosis [14]. This is encouraged by the recently published data on the *SOST* knock out mouse [15], which has increased bone mass, while having normal skeletal morphology. Structure/function analysis of Sclerostin will certainly facilitate development of such SOST inhibitors. In this study we present the structure of murine Sclerostin by solution NMR spectroscopy revealing that only the cystin-knot motif is structured. Functional assays confirm that the flexible termini are dispensable for SOST mediated Wnt3a inhibition.

Materials and methods

Recombinant protein expression and purification

Expression and purification in insect cells. Full-length murine SOST was cloned into the pBAC3 vector (Invitrogen) for expression in Sf9 insect cells. The construct consists of a gp64 signal sequence followed by thrombin-cleavable His_6 tag. Sf9 cells and Triex (Novagen) insect cells were cultured in IPL41 Medium (CloneTech) supplemented with 5% FCS (v/v) and 100 U/ml penicillin G, 100 μg/ml streptomycin at 27 °C. Recombinant baculovirus were produced by co-transfection of the transfer plasmid with linearized Bac3000 virus DNA (Novagen) according to manufacturer's protocol. For expression cells were transfected using a MOI of 5 and were subsequently cultivated for 4 days at 27 °C. The protein was captured by

* Corresponding author. Fax: +49 931 888 6158.
E-mail address: mueller@botanik.uni-wuerzburg.de (T.D. Mueller).

0006-291X/$ - see front matter © 2009 Elsevier Inc. All rights reserved.
doi:10.1016/j.bbrc.2009.01.062

metal ion affinity chromatography using Ni^{2+}–NTA as resin (Qiagen). Final purification was performed by cation exchange chromatography using CM Sepharose (GE Healthcare). Sclerostin was eluted using a linear gradient 0–1 M NaCl in 10 mM Hepes, pH 7.5.

Expression and purification in Escherichia coli. Full-length murine Sclerostin (mSOST) and truncated variants (mSOSTΔC, mSOSTΔNC) were cloned into the vector pET28b (Novagen). mSOSTΔC comprises Gln^1 to Arg^{144} and the variant mSOSTΔNC consists of Asn^{36} to Arg^{144}. All expression constructs consisted of the N-terminal His_6-tag followed by a thrombin cleavage site. Protein expression was performed using the *E. coli* strain Rosetta(DE3). Cells were grown at 37 °C to an OD_{600} of 0.6, expression was induced for 3 h by addition of 1 mM IPTG. Cells were harvested by centrifugation and lysed by sonification. Sclerostin was expressed in inclusion bodies, which were solubilized using 6 M guanidium–hydrochloride, 100 mM NaH_2PO_4, 10 mM Tris, pH 8.0, and 1/1000 (v/v) β-mercaptoethanol. The protein solution was concentrated to 20 mg/ml and refolding was performed by rapid dilution 1:100 into 2 M LiCl, 50 mM Tris, pH 8.0, 30 mM Chaps, 500 mM Arginine, 2 mM GSH, 1 mM GSSG. After refolding for 5 days at 4 °C, the refolded mSOST was purified by cation exchange chromatography using CM sepharose (GE Healthcare) as described above. Final purification was performed by reversed-phase HPLC (gradient 0.1% TFA in H_2O–100% Acetonitrile) using a C8 column (Macherey Nagel).

^{15}N-labeled and ^{15}N-/^{13}C-doubly labeled proteins were produced by expressing mSOST and variants thereof in M9 minimal medium supplemented with 0.5 g/L $^{15}NH_4Cl$ and 4 g/L $^{13}C_6$-glucose. For NMR studies, the N-terminal His_6-tag was cleaved using biotinylated 0.1 U/mg Thrombin (Novagen) and removing the protease subsequently by streptavidin agarose.

Cell culture and Wnt-reporter gene assay. HEK293TSA, L-mWnt3a cells (CRL-2647, ATCC), and L-cells (control cells) (CRL-2648, ATCC) were cultured at 37 °C and 5% CO_2 in DMEM (Invitrogen) containing 10% (v/v) FCS, 100 U/ml penicillin G, 100 μg/ml streptomycin (Invitrogen) and for L-mWnt3a expressing cells 0.4 μg/ml G418 sulphate (BioWest) was added. mWnt3a-conditioned and control media were produced according to the manufacturer's protocol.

HEK293TSA cells were seeded at a density of 1×10^5 cells/ml using a 24-well plate. After 24 h cells were transfected with 50 ng pSV β-Gal (Promega), 200 ng M50 Super8xTopFlash [16] (provided by Randall Moon) and 150 ng pEF6V5HisB (Invitrogen) using HEKFectin (Bio-Rad) according to manufacturer's protocol. After 24 h mSOST or variant proteins were added in different concentrations and 10% (v/v) of mWnt3a-conditioned or control medium was added. The cells were incubated for 24 h, the medium was removed and cells were lysed. β-Galactosidase activity was determined by *o*-nitrophenol-galactopyranoside conversion at 405 nm and luciferase activity was measured using the Promega luciferase assay kit. Experiments were conducted as duplicates.

NMR data acquisition and structure analysis. For NMR analysis mSOST proteins were dissolved at concentrations from 0.6 to 1 mM in 20 mM KH_2PO_4, pH 6.0, 50 mM NaCl, 5% (v/v) D_2O, 0.2% (w/v) NaN_3. NMR data were acquired at 27 °C employing Bruker Advance spectrometer operating at 600, 750, and 900 MHz proton frequencies and using triple-resonance, single-axis gradient cryoprobes. Data were processed using XwinNMR or TopSpin software, data analysis was performed using Aurelia (Bruker).

Backbone sequential assignments were obtained using a set of triple resonance experiments, i.e. CBCA(CO)NH, CBCANNH, HBHA(-CO)NH, HN(CA)CO, and HNCO [17]. Side chain assignments were obtained from H(C)(CO)NH-TOCSY, C(CH)(CO)NH-TOCSY experiments and two ^{13}C-edited experiments, HCCH-TOCSY, and HCCH-COSY [17]. Assignments for aromatic side chains were made in a 2D-NOESY spectrum. Complete resonance assignments could be obtained for 91 out of 113 residues, while the remaining residues could be assigned at least partially.

Distance data were derived from three heteronuclear 3D-NOESY spectra, including ^{15}N- and ^{13}C-HSQC-NOESY spectra and several 2D-NOESY spectra from different samples and field strength. NOESY crosspeaks were converted into distance ranges being divided into three classes, very strong, medium, and weak, resulting in restraints on upper distances of 2.5, 3.5, and 5.0 Å, respectively. Additional upper limit boundaries for the use of pseudo-atoms were added for methyl groups, aromatic ring protons and methylene protons with degenerate chemical shifts. Dihedral angle restraints were derived for backbone φ and ψ angles based on C^α, C^β, C', and H^α chemical shifts using the program TALOS [18].

Structure calculation was performed using XPLOR (NIH version 2.21) [19]. Structures were calculated employing a simulated annealing protocol. For the final coordinate ensemble, 100 structures were calculated of which 15 were chosen on the basis of lowest restraint violations. To obtain insights into the inherent flexibility of Sclerostin steady-state $^1H\{^{15}N\}$-heteronuclear NOE were measured at 27 °C and 600 MHz using proton saturation time of 3 s and a relaxation delay of 2 s. For the experiment without proton saturation the frequency was shifted to off-resonance.

Results and discussion

N- and C-termini of Sclerostin are flexible

We initially prepared full-length murine Sclerostin (mSOST) in Sf9 cells (Fig. 1A). The protein comprising Gln^1 to Tyr^{188} could be obtained from the supernatant of Sf9 cells. Staining via the Periodic Schiff Acid method confirmed the presence of glycosylation; mass spectrometry subsequently showed both *N*-glycosylation sites, Asn^{28} and Asn^{150}, to be linked to carbohydrates. Storage of full-length mSOST over several weeks at 4 °C resulted in partial proteolysis although the protein solution had a purity of $\geqslant$95%. Thus residual protease activity cleaves mSOST indicating the presence of flexible regions. The largest fragment showed an apparent molecular weight of roughly 10–12 kDa in a SDS–PAGE analysis (Fig. 1B). Mass spectrometry gave a molecular weight of 10,254 Da, which corresponds to a fragment comprising Glu^{52} to Cys^{142}. To test whether only the cystin-knot contains a rigid structure, we expressed a C-terminally truncated version of mSOST (mSOSTΔC: Gln^1 to Arg^{144}) in insect cells. This variant exhibits wildtype-like activity in a reporter gene assay measuring SOST-mediated Wnt3a inhibition indicating that the C-terminus is dispensable for activity. We further truncated mSOSTΔC by cleaving the protein by endopeptidase GluC. The resulting protein had a molecular weight of 12,266 Da as determined by ESI-FT-ICR mass spectrometry and comprised Asn^{36} to Arg^{144} (for further details regarding mass spectrometry analyses see Supplementary Fig. 1). The N- and C-terminally shortened mSOST still showed activity in the reporter gene assay although the IC_{50} shifted to slightly elevated concentrations (Data not shown).

Bacterial expression of mSOST for structure analysis

For structure analysis of Sclerostin we expressed mSOST in *E. coli*. Due to Sclerostin containing eight cysteines, which form four disulfides, soluble bacterial expression of mSOST seems difficult. We thus produced mSOST by expression into inclusion bodies and subsequent refolding. Murine SOST and the variants mSOSTΔC and mSOSTΔNC (Fig. 1A) could be nevertheless prepared in sufficient yields and purified to homogeneity (Fig. 1C). The full-length mSOST proteins derived from insect cells and bacteria exhibit iden-

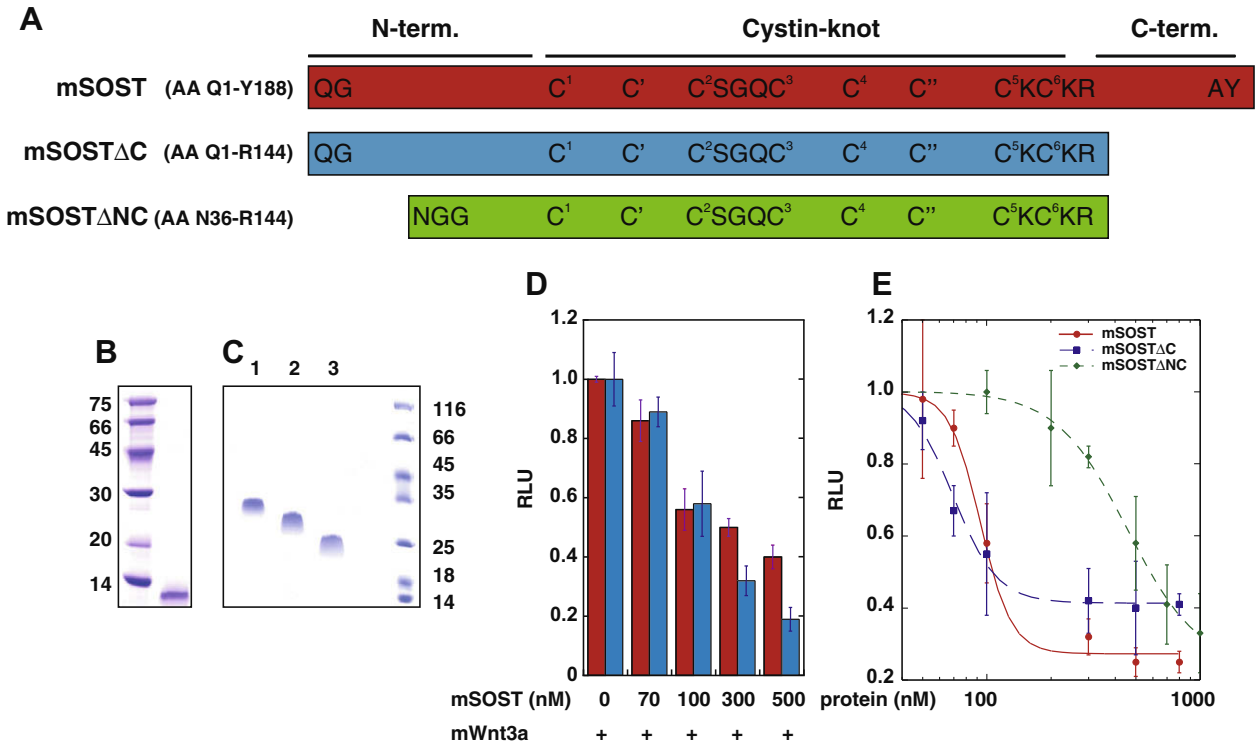

Fig. 1. (A) Expression constructs of mSOST: Gln^{1} to Tyr^{188}; mSOSTΔC: Gln^{1} to Arg^{144}; mSOSTΔNC: Asn^{36} to Arg^{144}. (B) SDS–PAGE of a proteolytically stable SOST fragment derived from Sf9-expressed mSOST after 60 days storage at 4 °C. (C) SDS–PAGE analysis of bacterially derived mSOST (1), mSOSTΔC (2) and mSOSTΔNC (3). (D) Inhibition of mWnt3a mediated luciferase expression by Sf9-derived full-length mSOST (red bars) and *E. coli*-derived mSOST (blue bars). (E) Inhibition of mWnt3a-mediated luciferase expression by bacterially derived mSOST (red curve) and truncation variants mSOSTΔC (blue) and mSOSTΔNC (green).

tical bioactivities (Fig. 1D and E). The N- and C-terminally shortened mSOSTΔNC, however, shows a slightly reduced activity indicating a possible requirement of the N-terminus of mSOST for maximal activity (Fig. 1E). To additionally test our hypothesis that the N- and C-terminus are highly flexible and unstructured we compared the 2D ^{1}H–^{15}N HSQC spectra of uniformly ^{15}N-labeled full-length mSOST and mSOSTΔNC. Residues located in the termini of mSOST exhibit amide proton chemical shift values between 7.5 and 8.5 ppm indicative for random coil conformation (Supplementary Fig. 2).

Overall architecture of Sclerostin

We determined the structure of the smallest construct termed mSOSTΔNC comprising Asn^{36} to Arg^{144}. Several residues showed broad NMR signals indicating flexibility on a slow-to-intermediate NMR time scale. Interestingly, many of these residues are part of or close to the cystin-knot suggesting that the knot is flexible to some degree. NOEs between backbone amide and Hα protons indicate two antiparallel β-sheet like structures running from His^{59} to Leu^{78}, now termed finger 1, and from Asp^{112} to Cys^{140} now referred to as finger 2. Whereas in finger 1 the interstrand NOE pattern is less regular and is disrupted between Thr^{61}-Arg^{62} and Lys^{73}-Pro^{74}, the NOEs in finger 2 suggest a regular antiparallel β-sheet. The region between residue Gly^{85} and Phe^{107}, termed loop, does not show a NOE pattern consistent with any typical secondary structure. Similarly only intraresidue and sequential NOEs are observed for the N-terminus (Asn^{36} to Lys^{48}) suggesting that the shortened N-terminus of mSOSTΔNC is still flexible and likely disordered. The deviations of the ^{13}C chemical shift of the Cα, Cβ, and carbonyl atoms from random coil values confirm this secondary structure analysis (Supplementary Fig. 3) [20,21].

NMR structure of mSclerostin

Thousand hundred and forty-three NOE-derived distance constraints were obtained from 2D- and heteronuclear 3D-NOESY spectra. Together with dihedral angle restraints for 87 residues derived from TALOS and Cα and Cβ carbon chemical shift restraints 100 structures were calculated of which 15 were selected on the basis of restraint violations and total energy (Supplementary Table 1). None of the structures exhibits systematic NOE restraint violations larger than 0.2 Å. The calculation reveals an extended structure with three "loops" emanating from the central cystin-knot (Cys^{55}-Cys^{109}, Cys^{80}-Cys^{140}, and Cys^{84}-Cys^{142}) (Fig. 2). Fingers 1 and 2 continue into the same direction from the knot and form an all-antiparallel β-sheet (Supplementary Fig. 4). The loop comprising residues Gly^{85} to Phe^{107} runs into the opposite direction and does not exhibit any regular secondary structure. A structure superposition shows that fingers 1 and 2 form the structured "core" of SOST exhibiting a rms deviation of about 0.7 Å for the backbone atoms (Supplementary Table 1). Finger 1 contains two short β-sheets, with β-strand 1 comprising His^{59} to Tyr^{60} and being antiparallel to β-strand 4 (Glu^{77} and Leu^{78}). The second β-sheet is located at the tip of finger 1 with β-strand 2 running from Thr^{65} to Asp^{66} and strand β3 from Cys^{69} to Arg^{70}. In finger 2 a long two-stranded sheet is formed with β-strand 5 running from Arg^{113} to Cys^{123}, the last two residues forming an antiparallel sheet with β-strand 3, and β-strand 6 composed of residues Arg^{130} to Ser^{139}. The disulfide between Cys^{69} (β-strand 3) and Cys^{123} (β-strand 5) connects both fingers thereby restraining the conformational flexibility.

Structural alignment using the residues of fingers 1 and 2 (Fig. 2) suggests that the loop is completely disordered, however, local fitting of residues Asn^{92} to Trp^{100} shows that the loop tip can adopt a partially ordered structure (Supplementary Fig. 5).

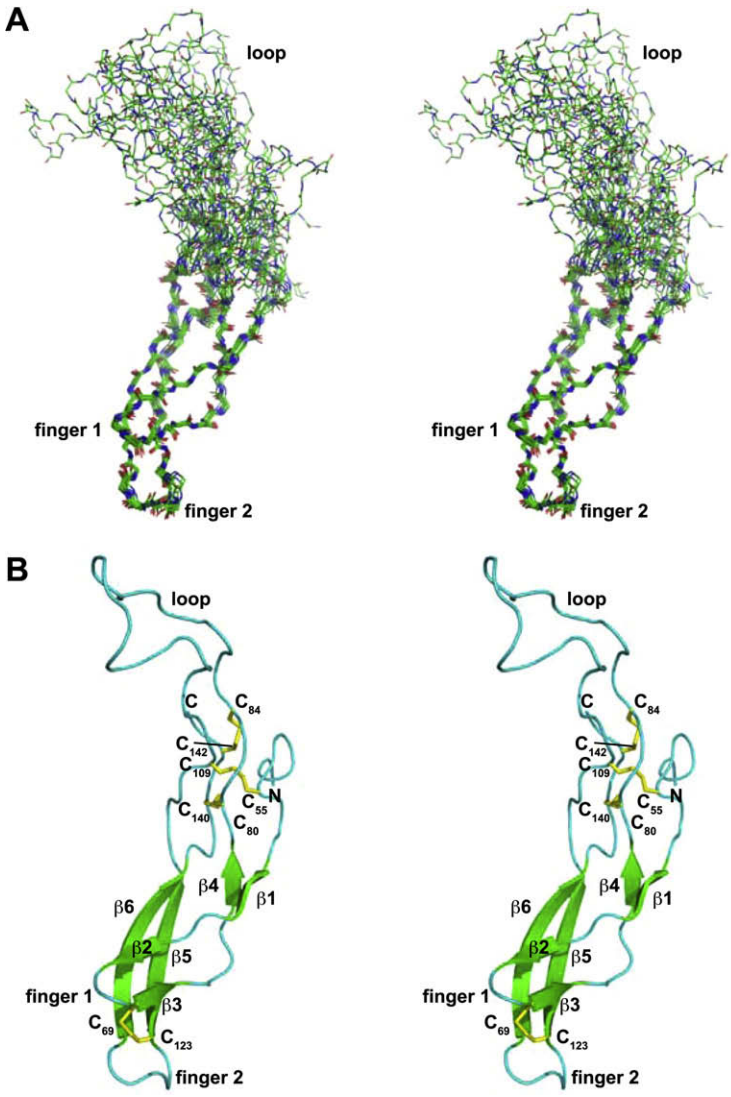

Fig. 2. (A) Stereoview of the backbone trace of 15 structures of mSOST superimposed on the Cα-atoms of residues 57–78 and 114–138. (B) Stereoview of a ribbon representation of a representative structure of the NMR ensemble. The secondary structure elements are indicated (see main text), the disulfide linkages are shown as sticks.

To ensure that the flexibility seen in mSOST is not due to an artificial lack of NOEs we measured $^{1}H\{^{15}N\}$-heteronuclear NOEs to determine flexibility directly (Fig. 3). The results confirm that the loop is less ordered and flexible, as all residues in this loop exhibit considerably smaller $^{1}H\{^{15}N\}$-NOEs compared to residues of the fingers. Similarly residues in the N-terminus also show smaller hetero-NOEs confirming that the terminus is highly dynamical.

A comparison of the mSOST structure using TOPMATCH [22] reveals very limited structural homology to other proteins. Due to the Structural restraints structures containing a cystin knot share a common architecture [23]. Thus structural homology is observed with BMP and Activin monomeric subunits (Supplementary Fig 6). However, the differences between the Cα-atom positions of BMPs and mSOST are large. Compared to BMPs, the cystin-knot of mSOST seems to exhibit a less rigid structure, possibly due to the differences in the flanking β-strand structures. In BMPs the residues C-terminal of the first knot cysteine are embedded in a regular β-sheet, the first two residues C-terminal of Cys^{55}, Arg^{56} and Glu^{57}, in mSOST, however, bulge out and do not form a regular β-sheet. Similarly, the structural equivalent of the mSOST loop in BMPs is the helix α1, which is embedded in the interdimer interface leading to stabilization of the cystin-knot. The highest structural similarity can be observed between SOST and the β-chain of the human chorionic gonadotropin (hCG). hCG, however, forms a non-covalently linked heterodimer consisting of an α- and β-chain, with the β-chain sharing a similar cysteine pattern and disulfide linkage with SOST (Supplementary Fig. 7).

Conclusion

Since the interaction of SOST and BMPs is currently under debate [7], the Wnt co-receptor LRP5 is so far the only confirmed interaction partner of SOST [10,11]. Although no complex structure of SOST bound to LRP5 is currently available, the structure of mSOST now provides a first possible interaction model. One hallmark of SOST is the high abundance of positively charged residues (34 Arg and Lys residues) resulting in a rather basic protein (pI_{calc} 9.6). The putative binding site of SOST on LRP5 is predicted in the first β-propeller due to mutations causing the High Bone Mass phenotype [13], which is highly similar to the SOST knockout phenotype [15]. Interestingly calculation of the electrostatic potential of SOST and LRP5 propeller 1 shows a remarkable complementary charge distribution with the putative binding site on LRP5 being

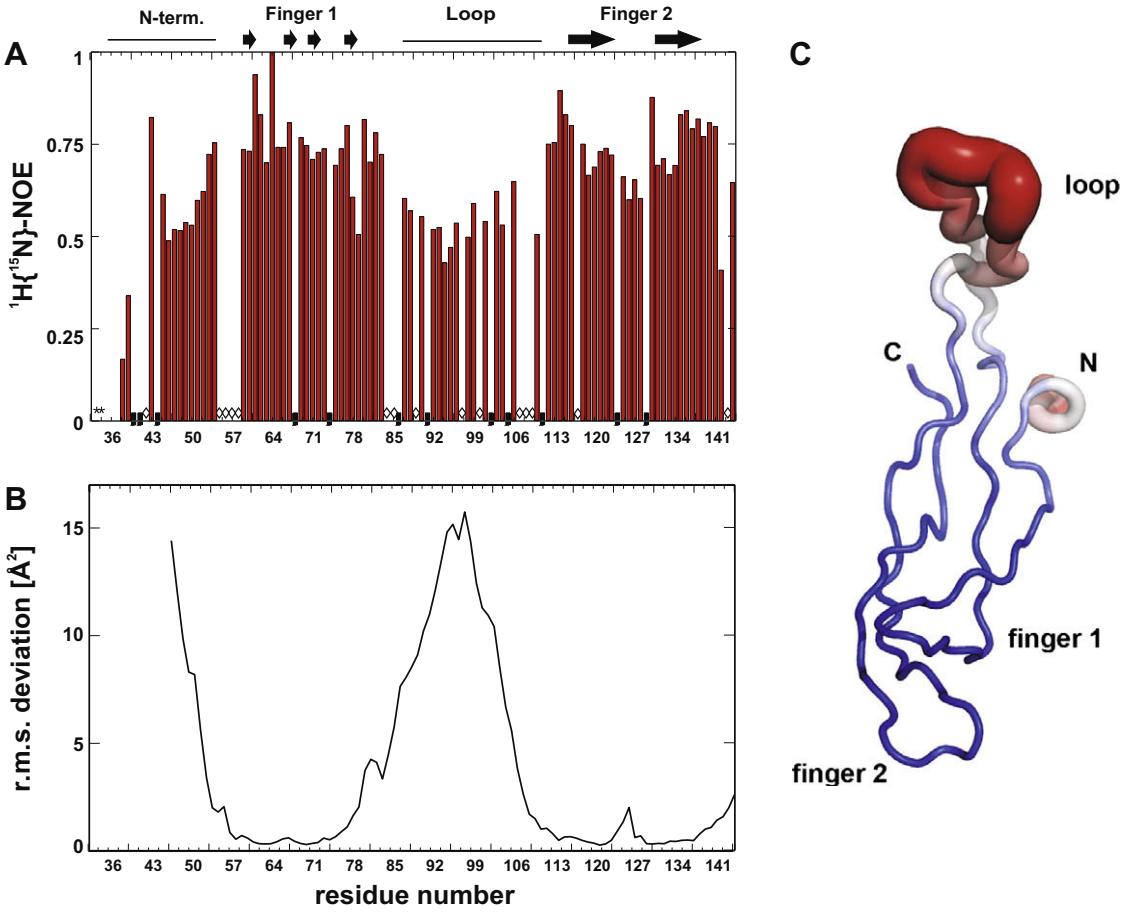

Fig. 3. (A) $^1H\{^{15}N\}$-hetero NOEs determined for mSOSTΔNC. Residues indicated with an asterisk exhibit no hetero-NOE, signals of residues marked by a diamond symbol could not be integrated, residues marked by a black bar are proline residues. (B) Plot of the rms deviation of the Cα-atom positions of the 15 individual NMR structures of mSOST (only residues 48–144) compared to the averaged non-minimized structure. (C) "Sausage" plot of the averaged minimized structure of mSOSTΔNC showing the highly flexible regions of mSOST. Regions colored in blue mark structurally highly defined areas, regions marked in red are highly disordered.

highly negatively charged and especially finger 2 of SOST exhibiting a strong positive electrostatic potential (Fig. 4). This observation suggests that finger 2 of SOST is the possible site of interaction with LRP5, further functional analyses using the now available structure for guidance are, however, required to test this hypothesis.

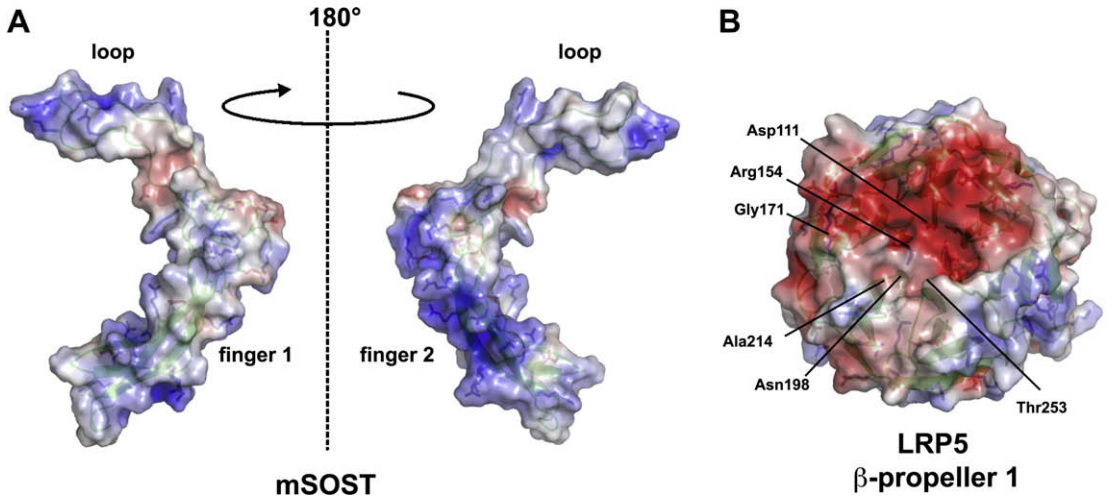

Fig. 4. (A) Electrostatic potential mapped onto the van der Waals surface of mSOST. Dark blue areas indicate a strongly positively charge potential at $5kT/e$, dark red areas mark negatively charged regions exhibiting an electrostatic potential of $-5kT/e$. The potentials were calculated using the software APBS employing an ionic strength of 0.15 M NaCl and the AMBER forcefield for protonation. (B) Electrostatic potential map analysis for the first propeller domain of human LRP5. The structure model for LRP5 was derived from Swiss-model, the calculation was performed as above. Residues in LRP5 mutated in diseases causing High Bone Mass are indicated.

Acknowledgments

Structure coordinates and NOE restraints of mSOST were deposited at the Protein Data Bank with the Accession Code 2KD3. The authors would like to thank Randal Moon for kindly providing the Wnt-reporter gene construct M50. This project was supported by the EU FP7 project TALOS.

Appendix A. Supplementary data

Supplementary data associated with this article can be found, in the online version, at doi:10.1016/j.bbrc.2009.01.062.

References

[1] S.A. Stein, C. Witkop, S. Hill, M.D. Fallon, L. Viernstein, G. Gucer, P. McKeever, D. Long, J. Altman, N.R. Miller, S.L. Teitelbaum, S. Schlesinger, Sclerosteosis: neurogenetic and pathophysiologic analysis of an American kinship, Neurology 33 (1983) 267–277.
[2] F.S. van Buchem, H.N. Hadders, R. Ubbensx, An uncommon familial systemic disease of the skeleton: hyperostosis corticalis generalisata familiaris, Acta Radiol. 44 (1983) 109–120.
[3] W. Balemans, N. Patel, M. Ebeling, E. van Hul, W. Wuyts, C. Lacza, M. Dioszegi, F.G. Dikkers, P. Hildering, P.J. Willems, J.B. Verheij, K. Lindpaintner, B. Vickery, D. Foernzler, W. van Hul, Identification of a 52 kb deletion downstream of the SOST gene in patients with van Buchem disease, J. Med. Genet. 39 (2002) 91–97.
[4] M.E. Brunkow, J.C. Gardner, J. van Ness, B.W. Paeper, B.R. Kovacevich, S. Proll, J.E. Skonier, L. Zhao, P.J. Sabo, Y. Fu, R.S. Alisch, L. Gillett, T. Colbert, P. Tacconi, D. Galas, H. Hamersma, P. Beighton, J. Mulligan, Bone dysplasia sclerosteosis results from loss of the SOST gene product, a novel cystine knot-containing protein, Am. J. Hum. Genet. 68 (2001) 577–589.
[5] W. Balemans, M. Ebeling, N. Patel, E. van Hul, P. Olson, M. Dioszegi, C. Lacza, W. Wuyts, J. van Den Ende, P. Willems, A.F. Paes-Alves, S. Hill, M. Bueno, F.J. Ramos, P. Tacconi, F.G. Dikkers, C. Stratakis, K. Lindpaintner, B. Vickery, D. Foernzler, W. van Hul, Increased bone density in sclerosteosis is due to the deficiency of a novel secreted protein (SOST), Hum. Mol. Genet. 10 (2001) 537–543.
[6] K.E. Poole, R.L. van Bezooijen, N. Loveridge, H. Hamersma, S.E. Papapoulos, C.W. Lowik, J. Reeve, Sclerostin is a delayed secreted product of osteocytes that inhibits bone formation, FASEB J. 19 (2005) 1842–1844.
[7] R.L. van Bezooijen, B.A. Roelen, A. Visser, L. van der Wee-Pals, E. de Wilt, M. Karperien, H. Hamersma, S.E. Papapoulos, P. ten Dijke, C.W. Lowik, Sclerostin is an osteocyte-expressed negative regulator of bone formation, but not a classical BMP antagonist, J. Exp. Med. 199 (2004) 805–814.
[8] D.G. Winkler, M.K. Sutherland, J.C. Geoghegan, C. Yu, T. Hayes, J.E. Skonier, D. Shpektor, M. Jonas, B.R. Kovacevich, K. Staehling-Hampton, M. Appleby, M.E. Brunkow, J.A. Latham, Osteocyte control of bone formation via sclerostin, a novel BMP antagonist, EMBO J. 22 (2003) 6267–6276.
[9] M.K. Sutherland, J.C. Geoghegan, C. Yu, E. Turcott, J.E. Skonier, D.G. Winkler, J.A. Latham, Sclerostin promotes the apoptosis of human osteoblastic cells: a novel regulation of bone formation, Bone 35 (2004) 828–835.
[10] X. Li, Y. Zhang, H. Kang, W. Liu, P. Liu, J. Zhang, S.E. Harris, D. Wu, Sclerostin binds to LRP5/6 and antagonizes canonical Wnt signaling, J. Biol. Chem. (2005).
[11] M. Semenov, K. Tamai, X. He, SOST is a ligand for LRP5/LRP6 and a Wnt signaling inhibitor, J. Biol. Chem. 280 (2005) 26770–26775.
[12] D.L. Ellies, B. Viviano, J. McCarthy, J.P. Rey, N. Itasaki, S. Saunders, R. Krumlauf, Bone density ligand, Sclerostin, directly interacts with LRP5 but not LRP5G171V to modulate Wnt activity, J. Bone Miner. Res. 21 (2006) 1738–1749.
[13] M.V. Semenov, X. He, LRP5 mutations linked to high bone mass diseases cause reduced LRP5 binding and inhibition by SOST, J. Biol. Chem. 281 (2006) 38276–38284.
[14] C. Deal, Potential new drug targets for osteoporosis, Nat. Clin. Pract. Rheumatol. 5 (2009) 20–27.
[15] X. Li, M.S. Ominsky, Q.T. Niu, N. Sun, B. Daugherty, D. D'Agostin, C. Kurahara, Y. Gao, J. Cao, J. Gong, F. Asuncion, M. Barrero, K. Warmington, D. Dwyer, M. Stolina, S. Morony, I. Sarosi, P.J. Kostenuik, D.L. Lacey, W.S. Simonet, H.Z. Ke, C. Paszty, Targeted deletion of the sclerostin gene in mice results in increased bone formation and bone strength, J. Bone Miner. Res. 23 (2008) 860–869.
[16] M.T. Veeman, D.C. Slusarski, A. Kaykas, S.H. Louie, R.T. Moon, Zebrafish prickle, a modulator of noncanonical Wnt/Fz signaling, regulates gastrulation movements, Curr. Biol. 13 (2003) 680–685.
[17] J. Cavanagh, Protein NMR Spectroscopy: Principles and Practice, Academic Press, San Diego, 1996.
[18] G. Cornilescu, F. Delaglio, A. Bax, Protein backbone angle restraints from searching a database for chemical shift and sequence homology, J. Biomol. NMR 13 (1999) 289–302.
[19] C.D. Schwieters, J.J. Kuszewski, G.M. Clore, Using Xplor-NIH for NMR molecular structure determination, Prog. Nucl. Magn. Reson. Spectrosc. 48 (2006) 47–62.
[20] D.S. Wishart, B.D. Sykes, The C-13 chemical-shift index – a simple method for the identification of protein secondary structure using C-13 chemical-shift data, J. Biomol. NMR 4 (1994) 171–180.
[21] D.S. Wishart, B.D. Sykes, F.M. Richards, The chemical shift index: a fast and simple method for the assignment of protein secondary structure through NMR spectroscopy, Biochemistry 31 (1992) 1647–1651.
[22] M.J. Sippl, M. Wiederstein, A note on difficult structure alignment problems, Bioinformatics 24 (2008) 426–427.
[23] O. Avsian-Kretchmer, A.J. Hsueh, Comparative genomic analysis of the eight-membered ring cystine knot-containing bone morphogenetic protein antagonists, Mol. Endocrinol. 18 (2004) 1–12.